

See discussions, stats, and author profiles for this publication at: <https://www.researchgate.net/publication/51633732>

# Quantum Chemistry Studies of Electronically Excited Nitrobenzene, TNA, and TNT

ARTICLE *in* THE JOURNAL OF PHYSICAL CHEMISTRY A · SEPTEMBER 2011

Impact Factor: 2.69 · DOI: 10.1021/jp204104j · Source: PubMed

---

CITATIONS

15

READS

51

## 5 AUTHORS, INCLUDING:



[Jason Quenneville](#)  
Spectral Sciences Incorporated  
33 PUBLICATIONS 1,146 CITATIONS

[SEE PROFILE](#)



[David S. Moore](#)  
Los Alamos National Laboratory  
188 PUBLICATIONS 2,333 CITATIONS

[SEE PROFILE](#)



[Shawn McGrane](#)  
Los Alamos National Laboratory  
75 PUBLICATIONS 498 CITATIONS

[SEE PROFILE](#)



[Jason Scharff](#)  
Los Alamos National Laboratory  
24 PUBLICATIONS 175 CITATIONS

[SEE PROFILE](#)

# Quantum Chemistry Studies of Electronically Excited Nitrobenzene, TNA, and TNT

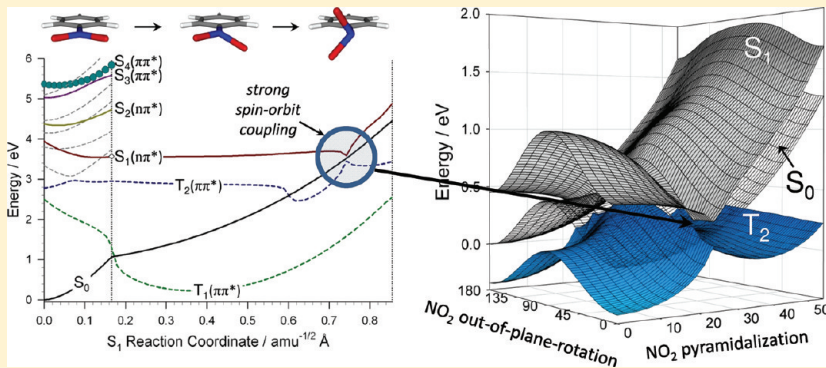
Jason Quenneville\*

Spectral Sciences, Inc., 4 Fourth Avenue, Burlington, Massachusetts 01803, United States

Margo Greenfield, David S. Moore, Shawn D. McGrane, and R. Jason Scharff

Shock and Detonation Physics Group, Los Alamos National Laboratory, Los Alamos, New Mexico 87545, United States

S Supporting Information

**ABSTRACT:**

The electronic excitation energies and excited-state potential energy surfaces of nitrobenzene, 2,4,6-trinitroaniline (TNA), and 2,4,6-trinitrotoluene (TNT) are calculated using time-dependent density functional theory and multiconfigurational ab initio methods. We describe the geometrical and energetic character of excited-state minima, reaction coordinates, and nonadiabatic regions in these systems. In addition, the potential energy surfaces for the lowest two singlet ( $S_0$  and  $S_1$ ) and lowest two triplet ( $T_1$  and  $T_2$ ) electronic states are investigated, with particular emphasis on the  $S_1$  relaxation pathway and the nonadiabatic region leading to radiationless decay of  $S_1$  population. In nitrobenzene, relaxation on  $S_1$  occurs by out-of-plane rotation and pyramidalization of the nitro group. Radiationless decay can take place through a nonadiabatic region, which, at the TD-DFT level, is characterized by near-degeneracy of three electronic states, namely,  $S_1$ ,  $S_0$ , and  $T_2$ . Moreover, spin–orbit coupling constants for the  $S_0/T_2$  and  $S_1/T_2$  electronic state pairs were calculated to be as high as  $60 \text{ cm}^{-1}$  in this region. Our results suggest that the  $S_1$  population should quench primarily to the  $T_2$  state. This finding is in support of recent experimental results and sheds light on the photochemistry of heavier nitroarenes. In TNT and TNA, the dominant pathway for relaxation on  $S_1$  is through geometric distortions, similar to that found for nitrobenzene, of a single ortho-substituted  $\text{NO}_2$ . The two singlet and lowest two triplet electronic states are qualitatively similar to those of nitrobenzene along a minimal  $S_1$  energy pathway.

**I. INTRODUCTION**

Active detection of high explosives signatures in the UV/vis spectral region is a promising area of research.<sup>1</sup> Our research focuses on stimulation of photoluminescence in high explosives through optimal control of wavepacket dynamics with shaped laser pulses.<sup>2,3</sup> Shaped UV/vis laser pulses might also be useful for the initiation of explosives, and detonators based on this technology could prove to be a safer and more secure alternative to those currently used. Theoretical studies are being used to map the UV/vis manifold of excited electronic state potential energy surfaces to help uncover control mechanisms, predict spectral signatures, and help explain experiments. Nitro-substituted benzene compounds comprise a significant fraction of common explosives.

Nitroarene excited states are important in environmental chemistry as well. Nitro-polycyclic aromatic hydrocarbons (NPAHs) are formed and released to the environment through incomplete combustion reactions and are understood to be both mutagenic and carcinogenic.<sup>4</sup> Photochemical degradation is the most common means for their natural removal.<sup>4</sup>

Past experimental and theoretical studies provide useful information on the photoluminescence of nitroarenes, but thus far, the description is incomplete. First, whereas benzene fluoresces

**Received:** May 3, 2011**Revised:** September 11, 2011**Published:** September 13, 2011

with a quantum yield of  $\sim 0.2$  in the gas phase,<sup>5</sup> most nitroaromatic compounds are known to be nonfluorescent.<sup>6</sup> On the other hand, it has long been known that strong spin–orbit coupling between the singlet and triplet states of nitroarenes can exist,<sup>7–9</sup> and ultrafast intersystem crossing (ISC) has been measured in a number of nitroarene compounds.<sup>6,10–14</sup> Phosphorescence has been detected in nitroarenes with larger aromatic (fused benzene) ring systems such as 1-nitronaphthalene.<sup>15</sup>

The present study focuses on three nitro-substituted benzene compounds (Scheme 1): nitrobenzene (NB), 2,4,6-trinitroaniline (TNA), and 2,4,6-trinitrotoluene (TNT). NB is the simplest nitroarene and therefore also the easiest to study with high-level quantum chemical methods. The dynamics of photoexcited solution-phase NB was studied experimentally by Takezaki et al.<sup>12,13</sup> Following excitation to the first singlet excited state ( $S_1$ ), an initial relaxation was measured with a time constant of 100 fs, followed by efficient ( $\phi = 0.8$ ) intersystem crossing from  $S_1$  to the second excited triplet excited state ( $T_2$ ) with a time constant of 6 ps. Rapid  $T_2 \rightarrow T_1$  internal conversion populates the lowest triplet state, which then decays to the singlet ground state with a time constant of 480 ps.<sup>12,13</sup> This  $T_1 \rightarrow S_0$  population conversion is unusually fast and is the basis for the absence of phosphorescence in NB.<sup>16</sup>

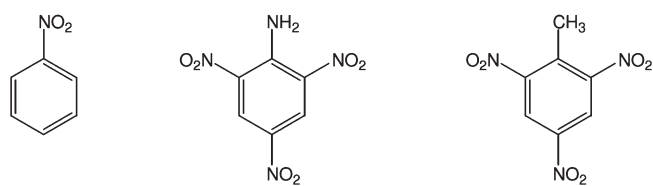
Although not widely used as such, TNA, also known as picramide, is a high explosive with a detonation velocity of 7.30 km/s.<sup>17</sup> TNA was chosen for study partly because it absorbs in the visible region of the spectrum, enabling experiments being conducted in tandem with the present theoretical study to be performed with a 400-nm pump laser. TNT is a common high explosive and has a detonation velocity of 6.90 km/s.<sup>17</sup> Its electronic absorption spectrum has been measured experimentally in the gas<sup>18</sup> and solution<sup>19</sup> phases. No UV/vis absorption spectrum of TNA was found in the literature, and to our knowledge, no previous theoretical studies of the global potential energy surfaces of either TNT or TNA excited states have been reported.

We have employed high-level theoretical techniques to gain a better understanding of the excited states and photochemical relaxation pathways of NB, TNA, and TNT. We used a combination of time-dependent density functional theory (TD-DFT) and multireference ab initio methods to calculate the electronic absorption spectra of these compounds and map their ground- and excited-state potential energy surfaces. We investigated excited-state minima, nonadiabatic regions, spin-orbit couplings, and pathways for both internal conversion and ISC. With the aid of previous studies, we aim to elucidate possible control routes for the photoluminescence and photodegradation of nitro-aromatic explosives, as well as to construct a basic model for nitroarene photochemistry that will serve as a tool for future studies.

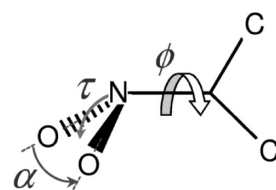
## II. METHODS

**Theoretical Work.** Ground-state geometries were optimized at the MP2 level of theory. Electronic absorption spectra were calculated in symmetry with the (linear-response) time-dependent density functional theory (TD-DFT) method, using the aug-cc-pVDZ basis set<sup>20</sup> and long-range corrected (LC) functionals, LC- $\omega$ PBE<sup>21–24</sup> (using Gaussian 09<sup>25</sup>) and LC-BLYP<sup>26–29</sup> (using Gaussian 03<sup>30</sup>). LC methods have been developed to correct the long-range behavior of the exchange-correlation energy functional. They are known to give improved excitation energy predictions for excited states with charge-transfer

**Scheme 1.** (Left to Right) Nitrobenzene (NB), 2,4,6-Trinitroaniline (TNA), and 2,4,6-Trinitrotoluene (TNT)



**Scheme 2.** Out-of-Plane Rotation,  $\phi$ , Pyramidalization,  $\tau$ , and Scissors,  $\alpha$ , Angles



character, states that are very important in nitroarenes. For all other TD-DFT calculations, either the cc-pVDZ<sup>20</sup> or the aug-cc-pVDZ basis set was used, and no symmetry restrictions were imposed.

Excited-state minimizations and conical intersection searches were performed with the cc-pVDZ basis set and the state-averaged complete-active-space self-consistent-field (CASSCF) method, abbreviated SA- $N$ -CAS( $n/m$ ), where  $n$  and  $m$  are the numbers of electrons and molecular orbitals, respectively, included in the active space. State averaging was used to avoid a variational bias of the wave function solution to the ground state; thus, the resultant wave function is an average over  $N$  electronic states. For excited-state geometry optimizations, we used an active space of 10 electrons in 8 orbitals and averaged over two states, SA-2-CAS(10/8). This active space, although admittedly smaller than optimal, was chosen to make conical intersection searches tractable. Single-point energies were calculated using larger active spaces, SA-2-CAS(12/11) and SA-2-CAS(16/13), as well as multiconfigurational perturbation theory (MCQDPT<sup>31,32</sup>) and TD-DFT. Because of the prohibitively large active spaces required to treat both the Franck–Condon region and the region of the  $S_1$  minimum, we did not compute the potential energy surfaces along the relaxation coordinate. Instead, a multireference treatment of the global energy surfaces is left for future work.

All optimizations were conducted using the Gaussian 03 quantum chemistry program.<sup>30</sup> Minimal-energy conical intersection searches were carried out using the method of Robb and co-workers.<sup>33–35</sup> TD-DFT calculations using the LC- $\omega$ PBE<sup>21–24</sup> and PBE0<sup>36</sup> density functionals were performed with Gaussian 03. MCQDPT calculations and TD-DFT calculations with the LC-BLYP<sup>28</sup> functional were carried out with the GAMESS quantum chemistry software.<sup>37,38</sup> Excited-state molecular dynamics (MD) simulations were performed with a home-grown computer code using the velocity Verlet integrator,<sup>39</sup> a time step of 0.125 fs, and Gaussian 03-computed forces.

Conical intersections of electronic states with like spin multiplicity were located, as described above, with CASSCF. Energies for triplet states were also computed in these regions using TD-DFT. Several qualitative deficiencies of the TD-DFT formalism (see refs 40 and 41 for reviews) were identified in a previous

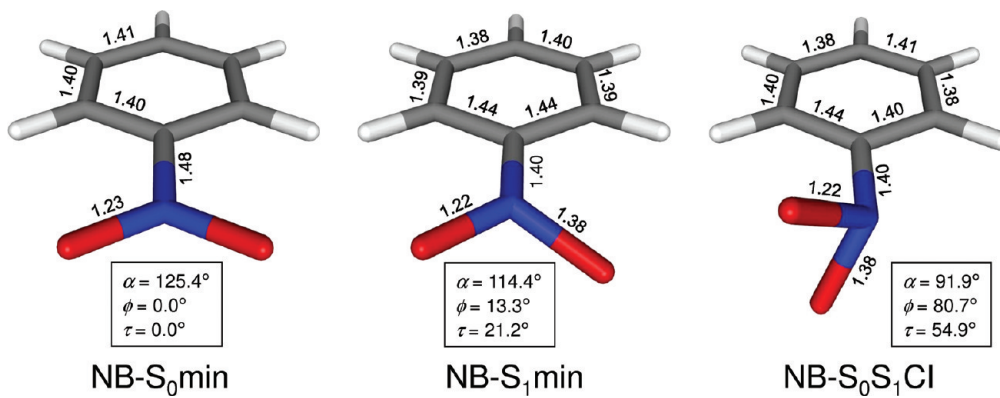


**Figure 1.** Molecular structures at the minima on the ground and first excited states and the minimum-energy  $S_0/S_1$  conical intersection in nitrobenzene. The ground-state structure was optimized in  $C_{2v}$  symmetry. Bond lengths are given in angstroms. The torsion ( $\phi$ ) and pyramidalization ( $\tau$ ) angles of the nitro group are described in Scheme 2.

**Table 1.** Electronic Excitation Energies ( $\Delta E$ ) and Oscillator Strengths ( $f$ ) of Nitrobenzene<sup>a–d</sup>

character	TD-LC- $\omega$ PBE <sup>e</sup>		TD-LC-BLYP <sup>e</sup>		CASPT2 <sup>f</sup>		$\Delta E$ (eV)	$f$	expt <sup>g</sup>	$\Delta E$ (eV)
	$\Delta E$ (eV)	$f$	$\Delta E$ (eV)	$f$	$\Delta E$ (eV)	$f$				
$^3B_2$ ( $T_1$ )	$\pi\pi^*$	2.50	0	2.86	0	3.31	0			
$^3A_1$ ( $T_2$ )	$n\pi^*$	2.78	0	3.32	0	3.62	0			
$^3A_2$	$\pi\pi^*$	3.34	0	3.29	0	3.36	0			
$^3B_1$	$n\pi^*$	3.80	0	3.79	0	3.97	0			
$^1A_2$ ( $S_1$ )	$n\pi^*$	3.94	0.000	3.84	0	3.57	0	3.65	0.003	>3.0
$^3B_2$	$\pi\pi^*$	4.15	0	4.12	0	4.16	0			
$^1B_1$ ( $S_2$ )	$n\pi^*$	4.38	0.004	4.31	0	4.14	0	4.38	0.01	
$^3A_1$	$\pi\pi^*$	4.46	0	4.46	0	4.23	0			
$^1B_2$ ( $S_3$ )	$\pi\pi^*$	5.03	0.018	4.86	0.018	4.40	0.004			
$^3B_2$	$\pi\pi^*$	5.10	0	5.08	0	5.86	0			
$^1A_1$ ( $S_4$ )	$\pi\pi^*$	5.36	0.209	5.16	0.218	4.99	0.193	5.17	0.17	4.62
$^3A_1$	$\pi\pi^*$	6.09	0	5.94	0	5.87	0			
$^1B_2$	$\pi\pi^*$	6.26	0.011	6.11	0.001	5.59	0.029	6.14	?	5.8
$^1A_1$	$\pi\pi^*$	6.70	0.349	6.57	0.289	6.20	0.425	6.42	0.38	6.3
$^1B_2$	$\pi\pi^*$	6.74	0.328	6.50	0.241	6.34	0.441			
$^3B_2$	$\pi\pi^*$	6.88	0	6.66	0	6.12	0			
$^3A_2$	$\sigma\pi^*$	7.05	0	6.78	0	6.14	0			
$^1A_2$	$\sigma\pi^*$	7.33	0.000	6.98	0.000	6.35	0.018			

<sup>a</sup> Symmetry restricted to  $C_{2v}$  for all but the CASCF and the MCQDPT calculations. <sup>b</sup> CASPT2 calculations taken from ref 46. <sup>c</sup> Character and ordering of the states taken from the TD-LC-BLYP calculations. <sup>d</sup> Results for triplet states given in italics. <sup>e</sup> aug-cc-pVDZ basis set. <sup>f</sup> From ref 46; CAS(18/13) wave function, polarized atomic natural orbital (ANO) basis set, geometry optimized with B3LYP/6-31G(d). <sup>g</sup> Gas phase, refs 47 and 48. <sup>h</sup> Solid film, ref 46.

study that can lead to inaccurate predictions in nonadiabatic regions.<sup>42</sup> First, linear-response TD-DFT does not treat double excitations correctly; therefore, conical intersection predictions involving states with double-excitation character are generally unreliable. Second, the dimensionality of a conical intersection (i.e., the dimensionality of the degenerate space) should be  $N - 2$ , however the dimensionality of the TD-DFT result is  $N - 1$  because of the diabatic nature of the TD-DFT states. Finally, the energy of the potential surfaces in the vicinity of a conical intersection varies much more rapidly in the TD-DFT result than in the state-averaged CASSCF result. Nevertheless, despite some qualitative shortcomings of the predictions, TD-DFT has been found to predict the presence and location of nonadiabatic regions quite accurately,<sup>42</sup> and the spin-flip DFT approach shows

promise in overcoming some of the inaccuracies found for other compounds.<sup>42,43</sup>

Spin-orbit couplings were calculated at the minimal-energy conical intersections using multireference configuration interaction (MRCI) and the full Pauli–Breit Hamiltonian as implemented in GAMESS.<sup>44,45</sup> In these calculations, the reference wave function was computed with SA-4-CAS(12/11), averaging over the  $S_0$ ,  $S_1$ ,  $T_1$ , and  $T_2$  states. The 1s core orbitals were frozen in the MRCI calculations.

A few important angles discussed throughout this article are depicted in Scheme 2. The O–N–O (scissors) bond angle is given as  $\alpha$ . The NO<sub>2</sub> rotation angle,  $\phi$ , is the angle made by the plane of the NO<sub>2</sub> group with the plane of the benzene ring. The pyramidalization angle,  $\tau$ , is the angle between the C–N bond vector and the plane of the NO<sub>2</sub> group.

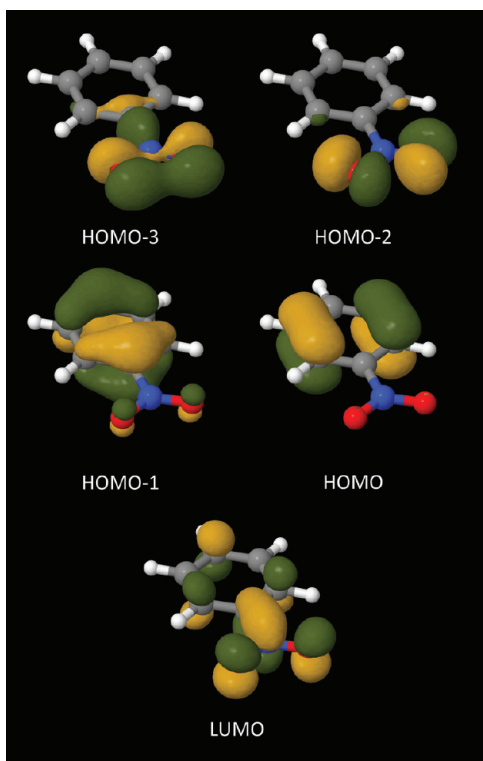


**Figure 2.** Two highest occupied and two lowest unoccupied molecular orbitals for the NB-S<sub>0</sub>Min structure, calculated with the LC-BLYP density functional method and the aug-cc-pVDZ basis set.

**Experimental Work.** The experimental visible absorption spectra of TNA were measured in the solid phase and in dilute acetone solution. The spectra were obtained with an Agilent UV/visible spectrophotometer (model 8453) equipped with a Labsphere diffuse reflectance accessory (model RSA-HP-8453), which measures both the specular and diffuse components of the reflectance. Experimental values for the excitation energies of nitrobenzene<sup>46–48</sup> and TNT<sup>18,19</sup> were taken from spectra found in the literature.

### III. RESULTS AND DISCUSSION

**Nitrobenzene.** The electronic excitation energies of ground-state nitrobenzene (NB-S<sub>0</sub>min, Figure 1), both calculated and experimental, are reported in Table 1. Our TD-DFT results are in good agreement with experimental<sup>47,48</sup> and LS-CASPT2<sup>46</sup> results. The first two singlet excited states are of  $n\pi^*$  type, and the lowest-energy  $\pi\pi^*$  states are S<sub>3</sub> and S<sub>4</sub>. Molecular orbitals (three occupied and one unoccupied) obtained from a TD-LC-BLYP/aug-cc-pVDZ calculation at the ground-state equilibrium geometry agree qualitatively with the findings of previous calculations<sup>49</sup> and are shown in Figure 2. The S<sub>0</sub> → S<sub>1</sub> transition involves promotion of an electron from the HOMO – 2 to the LUMO; S<sub>0</sub> → S<sub>2</sub> is HOMO – 3 → LUMO, and S<sub>0</sub> → S<sub>3</sub> is HOMO → LUMO. The lowest bright transition, S<sub>0</sub> → S<sub>4</sub>, is HOMO – 1 → LUMO. S<sub>4</sub>, which is often called the charge-transfer (<sup>1</sup>CT) state, is only slightly higher (0.3 eV) in energy than S<sub>3</sub> but has an oscillator strength at least an order of magnitude larger. Additionally, there are several triplet states lower than S<sub>4</sub> that, given the abnormally strong spin-orbit coupling in nitroarenes, need to be considered when pondering the possible decay pathways of photoexcited nitrobenzene.

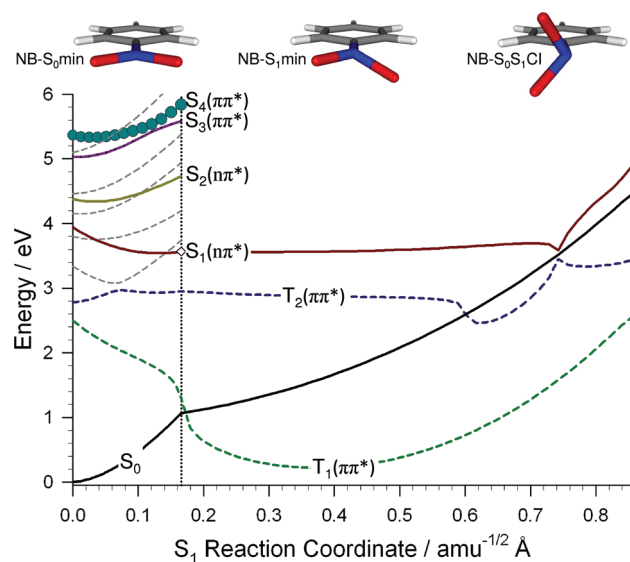


**Figure 3.** Energies (TD-LC- $\omega$ PBE/cc-pVDZ) of the lowest four singlet (solid lines) and lowest seven triplet (dashed lines) states in nitrobenzene along a linearly interpolated RC connecting the ground-state (S<sub>0</sub>) minimum, the S<sub>1</sub> minimum, and the S<sub>0</sub>/S<sub>1</sub> conical intersection, which are detailed in Figure 1. Vertical dotted lines mark the positions of the latter two structures along the RC. The first and second excited triplet states are drawn in green and blue, respectively, with the remaining triplet states shown in gray. Filled circles accompanying each line are weighted according to the oscillator strength of the transition between the given state and S<sub>0</sub>. The complete absence of a filled circle indicates a dark transition, which is the case for both the triplet states and the  $n\pi^*$  singlet states. The fact that S<sub>2</sub>, S<sub>3</sub>, and S<sub>4</sub> all increase in energy along the RC suggests that S<sub>4</sub> → S<sub>3</sub> → S<sub>2</sub> → S<sub>1</sub> population transfer occurs along a reaction that does not include a large degree of either pyramidalization or torsion of the NO<sub>2</sub> group.

The energy minimum on the S<sub>1</sub> state, NB-S<sub>1</sub>Min, is shown in Figure 1. The results of our SA-2-CAS(10/8) optimization are in very good agreement with the structure obtained by Takezaki et al.<sup>49</sup> using the state-specific CAS(12/11) method and a double- $\zeta$  basis set. In our smaller active space, there are one nonbonding orbital, four  $\sigma$  orbitals, and three  $\pi^*$  orbitals. The nitro group in this structure is slightly twisted out of the plane of the benzene ring and is also slightly pyramidalized. In addition, the O–N–O scissors angle closes by 11°, and the NO bonds differ in length by 0.16 Å.

We searched for a conical intersection in the vicinity of this minimum. The optimized minimal-energy conical intersection (denoted NB-S<sub>0</sub>S<sub>1</sub>CI and pictured in Figure 1) has a structure similar to that of the S<sub>1</sub> minimum, but the scissors, out-of-plane twist, and pyramidalization angles of the NO<sub>2</sub> group are all more pronounced. The S<sub>0</sub>–S<sub>1</sub> energy gap at this point was calculated to be 0.063 eV at the SA-2-CAS(10/8)/cc-pVDZ level. Table 2 lists the energy of this structure relative to the S<sub>1</sub> equilibrium geometry computed with larger CAS sizes, higher correlation methods, and TD-DFT, for each of the three compounds studied here. At the highest level of theory applied (MCQDPT), the NB-S<sub>0</sub>S<sub>1</sub>CI structure is 2.5 eV uphill in energy from NB-S<sub>1</sub>Min, but the S<sub>0</sub>–S<sub>1</sub> energy gap is 0.4 eV, suggesting that the nonadiabatic region has shifted in nuclear coordinate space and, thus, that this relative energy is overestimated. As a result, we regard the SA-2-CAS(16/13)-calculated S<sub>0</sub>S<sub>1</sub>CI – S<sub>1</sub>Min energy differences as our most accurate.

**Table 2.** Relative Energies (eV) and Electronic State Energy Gaps (eV) for the  $S_1$  Minima and  $S_0/S_1$  Conical Intersections of NB, TNA, and TNT<sup>a</sup>

	method												
	CAS(12/11) <sup>b</sup>			CAS(12/11)*PT <sup>b</sup>			CAS(16/13) <sup>b</sup>			TD-LC- $\omega$ PBE <sup>c</sup>			
	$E_{\text{gap}}^{\text{S}1 \text{ mind}}$	$E_{\text{gap}}^{\text{CI } e}$	$E_{\text{ref}}^{\text{b } f}$	$E_{\text{gap}}^{\text{S}1 \text{ mind}}$	$E_{\text{gap}}^{\text{CI } e}$	$E_{\text{ref}}^{\text{b } f}$	$E_{\text{gap}}^{\text{S}1 \text{ mind}}$	$E_{\text{gap}}^{\text{CI } e}$	$E_{\text{ref}}^{\text{b } f}$	$E_{\text{gap}}^{\text{S}1 \text{ mind}}$	$E_{\text{gap}}^{\text{CI } e}$	$E_{\text{ref}}^{\text{a } g}$	$E_{\text{ref}}^{\text{b } f}$
NB	2.08	0.06	1.12	2.49	0.33	1.28	1.78	0.02	0.50	2.84	0.07	-0.40	0.04
TNA	1.05	0.03	1.01	1.89	0.20	0.96	1.05	0.03	1.01	2.49	0.09	-0.27	0.37
TNT	1.31	0.05	0.48	2.28	0.74	1.22	1.31	0.02	0.58	2.62	0.13	-0.46	0.02

<sup>a</sup> MCQDPT calculations performed with GAMESS using the default settings. <sup>b</sup> CAS and CAS\*PT values were obtained from singlet-point calculations performed on the SA-2-CAS(10/8)/cc-pVDZ-optimized structures. <sup>c</sup> For TD-LC- $\omega$ PBE, energies for the  $S_1$  minima and  $S_0/S_1$  conical intersections taken as the lowest  $S_1$  energy and the  $S_1$  energy at the crossing point, respectively, from the linearly interpolated RC calculations shown in Figures 2, 8, and 11. <sup>d</sup>  $S_0 - S_1$  electronic energy gap at the  $S_1$  minimum. <sup>e</sup>  $S_0 - S_1$  electronic energy gap at the  $S_0/S_1$  conical intersection. <sup>f</sup>  $S_1$  energy of the conical intersection relative to the  $S_1$  minimum. <sup>g</sup>  $S_1$  energy of the  $S_1$  minimum relative to the  $S_0$  minimum.

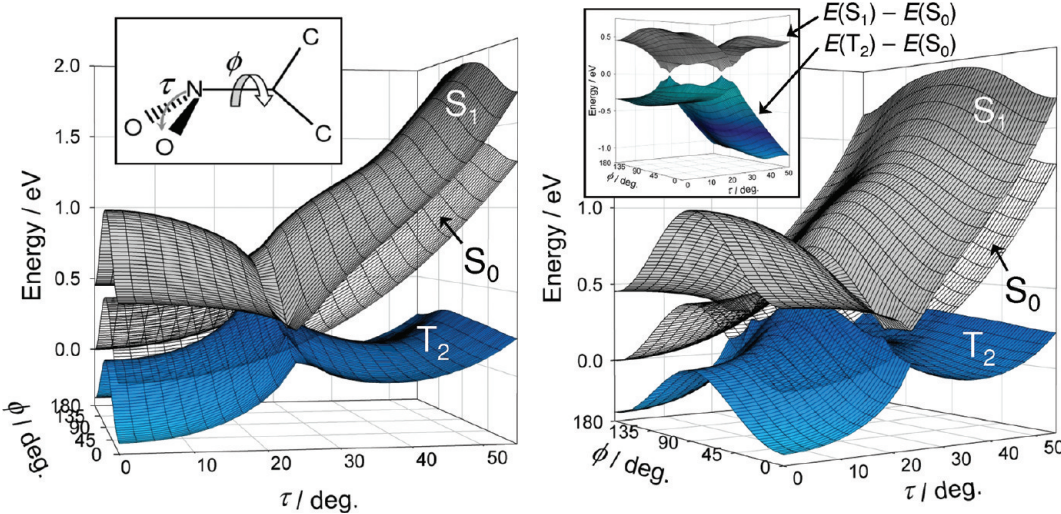


**Figure 4.** Two perspectives of reduced-space potential surfaces surrounding the three-state ( $T_2/S_0/S_1$ ) degeneracy of nitrobenzene, calculated with the TD-PBE0/cc-pVDZ method. The two coordinates that were varied are the out-of-plane rotation of the  $\text{NO}_2$  group,  $\phi$ , and its pyramidalization,  $\tau$ . All other coordinates were fixed at the values of the NB- $S_0$ Min structure, except the C–N and N–O bond lengths and the O–N–O bond angle, which were set to the values of NB- $S_0$ S<sub>1</sub>CI. The second inset is the electronic energy gap surfaces with the same perspective as shown in the right panel.

**Table 3.** Spin–Orbit Coupling Constants ( $\text{cm}^{-1}$ ) between Electronic States at the  $S_0S_1\text{CI}$  Geometries Singlet and Triplet<sup>a</sup>

	$S_0/T_2$	$S_1/T_2$
NB	26.39	53.02
TNA	15.60	60.13
TNT	25.69	50.44

<sup>a</sup> The SO-Cl method in GAMESS<sup>37,38</sup> was used with an SA-4-CAS(12/11) wave function, and the cc-pVDZ basis set

In Figure 3, we trace the potential energy of the lowest five singlet and lowest seven triplet states along an approximate reaction coordinate (RC) leading from the ground-state minimum to the  $S_1$  minimum and then to the conical intersection of  $S_0$  and  $S_1$ . Intermediate structures along the approximate RC were obtained through linear interpolation between these successive structures. It is important to note that all of the states shown in Figure 3 were calculated at the same geometries; thus, only the  $S_1$  energy curve is of minimal energy, and the other

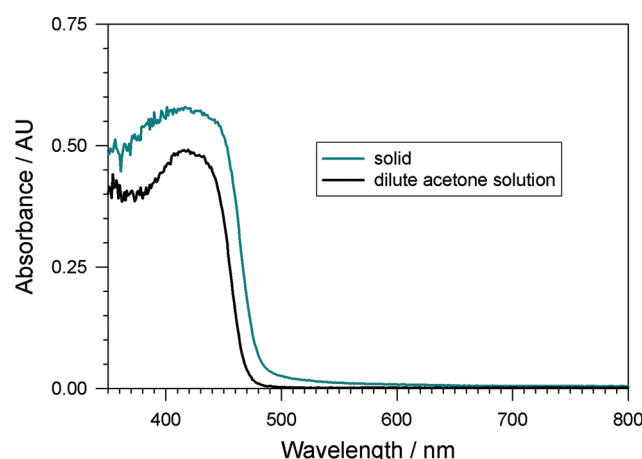


**Figure 5.** Experimental absorption spectra of TNA.

curves do not necessarily (and often do not) represent a relaxation pathway for the given adiabatic state. TD-DFT, which was used to calculate the energy in this plot, captures the nonadiabatic region at an intermediate geometry and,

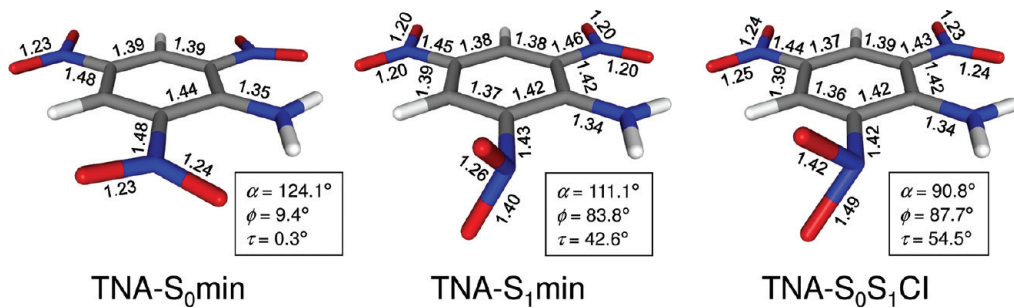


**Figure 6.** Molecular structures at the minima on the ground and first excited states and the minimum-energy  $S_0/S_1$  conical intersection in TNA. The ground-state structure was optimized in  $C_{2v}$  symmetry. Bond lengths are given in angstroms. The torsion ( $\phi$ ) and pyramidalization ( $\tau$ ) angles of the nitro group are described in Scheme 2.

**Table 4. Electronic Excitation Energies ( $\Delta E$ ) and Oscillator Strengths ( $f$ ) of 2,4,6-Trinitroaniline (TNA)<sup>a–c</sup>**

character	TD-LC- $\omega$ PBE <sup>d</sup>		TD-LC-BLYP <sup>d</sup>		CASSCF <sup>e</sup>	MCQDPT <sup>e</sup>	expt
	$\Delta E$ (eV)	$f$	$\Delta E$ (eV)	$f$			
$^3B_2$ ( $T_1$ )	$\pi\pi^*$	2.55	0	2.83	0		
$^3A_1$ ( $T_2$ )	$\pi\pi^*$	2.61	0	2.91	0		
$^3B_2$	$\pi\pi^*$	2.62	0	2.91	0		
$^3A_1$	$\pi\pi^*$	2.91	0	3.15	0		
$^3B_2$	$\pi\pi^*$	3.09	0	3.09	0		
$^3A_2$	$n\pi^*$	3.42	0	3.37	0		
$^3B_1$	$n\pi^*$	3.43	0	3.38	0		
$^3A_2$	$n\pi^*$	3.46	0	3.41	0		
$^3A_1$	$\pi\pi^*$	3.86	0	3.82	0		
$^1B_2$ ( $S_1$ )	$\pi\pi^*$	3.89	0.180	3.68	0.167	4.42	3.03
$^3B_1$	$n\pi^*$	3.89	0	3.87	0		$3.0^f$
$^3B_1$	$n\pi^*$	3.94	0	3.92	0		$3.0^g$
$^3A_2$	$n\pi^*$	3.97	0	3.96	0		$3.02^h$
$^1B_1$ ( $S_2$ )	$n\pi^*$	4.02	0.000	3.91	0.000		
$^1A_2$	$n\pi^*$	4.02	0.000	3.91	0.003		
$^1A_2$	$n\pi^*$	4.05	0.000	3.94	0.001		
$^1B_1$	$n\pi^*$	4.46	0.000	4.39	0.000		
$^1B_1$	$n\pi^*$	4.49	0.001	4.40	0.001		
$^3A_1$	$\pi\pi^*$	4.51	0	4.31	0		
$^1A_2$	$n\pi^*$	4.53	0.000	4.46	0.001		
$^1A_1$	$\pi\pi^*$	4.77	0.082	4.59	0.045		
$^1A_1$	$\pi\pi^*$	5.08	0.298	4.78	0.288		
$^3B_2$	$\pi\pi^*$	5.33	0	5.21	0		
$^3B_2$	$\pi\pi^*$	5.42	0	5.25	0		
$^1A_1$	$\pi\pi^*$	5.84	0.101	5.56	0.142		
$^1B_2$	$\pi\pi^*$	5.92	0.202	5.64	0.174		
$^3A_1$	$\pi\pi^*$	6.06	0	5.84	0		
$^3B_1$	$n\pi^*$	6.58	0	6.00	0		

<sup>a</sup> Symmetry restricted to  $C_{2v}$  for all but the CASSCF and the MCQDPT calculations. <sup>b</sup> Character and ordering of the states taken from the TD-LC-BLYP calculations. <sup>c</sup> Results for triplet states given in italics. <sup>d</sup> aug-cc-pVDZ basis set. <sup>e</sup> SA-2-CAS(12/11) wave function, cc-pVDZ basis set. <sup>f</sup> Dilute acetone solution, this work. <sup>g</sup> Solid phase, this work. <sup>h</sup> 2,4,6-Trinitro-N-ethylaniline in ethanol solution; ref 19.

therefore, with less  $\text{NO}_2$  distortion than in the CAS-optimized structure of Figure 1. Relative energies on  $S_1$  derived from this study are also given in Table 2. The  $S_0\text{S}_1\text{Cl} - S_1\text{Min}$  energy differences obtained with this method were found to be less than one-half the value predicted with CASSCF (Table 2).

The most interesting aspect of the  $S_0/S_1$  nonadiabatic region is the presence of a third near-degenerate state at the crossing point. The apparent confluence of the  $T_2$ ,  $S_0$ , and  $S_1$  states seen in our linearly interpolated RC plots could be erroneous. A higher level of theory might show that there are simply two intersection seams close to one another. Although three-state conical

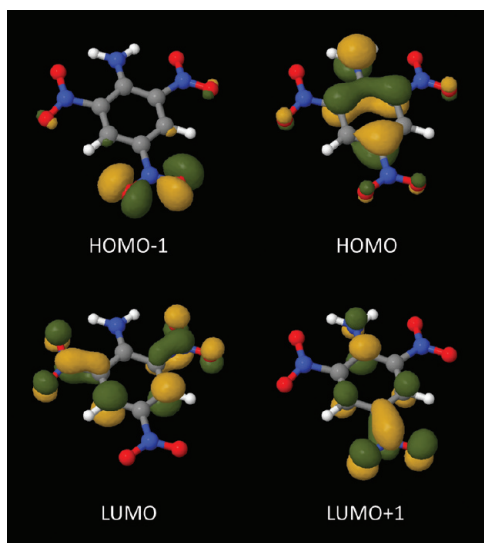


**Figure 7.** Two highest occupied and two lowest unoccupied molecular orbitals for the TNA- $S_0$ Min structure, calculated with the LC-BLYP density functional method and the aug-cc-pVDZ basis set.

intersections have been located in several molecules, including malonaldehyde and the DNA bases,<sup>50–55</sup> three-state intersections involving multiple spin states are not known to exist. To confirm that a nonadiabatic region is a conical intersection of three states, all three states must be optimized simultaneously.<sup>56</sup> In addition, intersections of states with unlike spin require treatment of spin–orbit coupling.<sup>57</sup> A more rigorous treatment is planned for the future, but for now, we discuss the potential energy surface topographies at a lower level and present a preliminary study of the spin–orbit coupling constants thereafter.

An intersection of  $S_1$  and  $T_2$  alone would help explain the experimental finding of picosecond  $T_2 \rightarrow S_1$  ISC; however, the fact that this is a nonadiabatic region involving three states complicates its interpretation. To investigate the electronic state topographies in this region, we calculated  $S_0$ ,  $S_1$ , and  $T_2$  along both the  $\text{NO}_2$  twist and pyramidalization coordinates. (Degeneracy of the electronic states is also believed to be influenced by the  $\text{O}-\text{N}-\text{O}$  scissors angle,  $\alpha$ , as well as elongation of one of the  $\text{N}-\text{O}$  bonds. See Figure 1 and Scheme 2.) The two-dimensional energy plots (Figure 4) reveal a sharp variation in the energy along the pyramidalization coordinate. The TD-DFT method has been shown to overestimate surface gradients in the vicinity of conical intersections compared to multi-reference methods;<sup>42</sup> nevertheless,  $\text{NO}_2$  pyramidalization appears to be important to energy gap closure for this NB nonadiabatic region. A seam of low electronic energy gap exists among the three states along the  $\text{NO}_2$  rotation angle, suggesting that access to the nonadiabatic region is independent of out-of-plane  $\text{NO}_2$  rotation.

To model the nonadiabatic wavepacket dynamics of NB, multistate MD calculations with an accurate treatment of spin–orbit coupling are required. In the absence of MD simulations, we made use of the work of Yarkony, who studied the topographies of conical intersections and how they can be used to predict wavepacket dynamics.<sup>58</sup> The funnel-like shape of the upper surface ( $S_1$ ) suggests that, when the wavepacket reaches this region, it will quickly funnel down to the lower state. In the present situation, there are two lower states that are degenerate. An upside-down funnel shape for the lower state (such as for  $T_2$ )

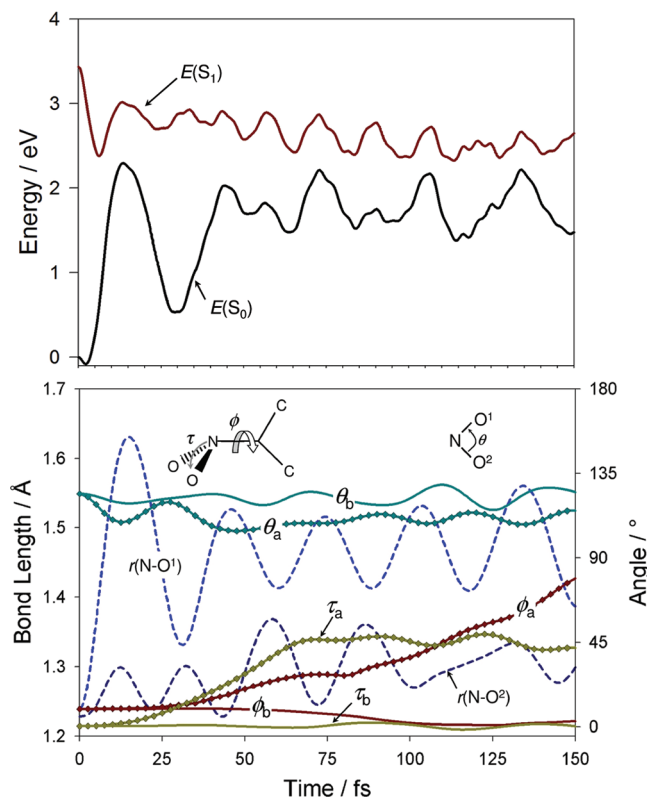


**Figure 8.** Results of an excited-state MD trajectory of TNA initiated at the  $S_0$  minimum on the  $S_1$  electronic state and computed using the SA-2-CAS(8/7)/6-31G method. (Top)  $S_0$  (black line) and  $S_1$  (red line) potential energies plotted as a function of time along an MD trajectory propagated on the  $S_1$  state of TNA. (Bottom) Time evolution of important geometrical parameters along the trajectory. In the labels, the a and b subscripts indicate the ortho-attached  $\text{NO}_2$  group to which the data pertain. One of the  $\text{N}-\text{O}$  bonds stretches within 15 fs to 1.6 Å and then oscillates about 1.45 Å. The  $\text{NO}_2$  group quickly pyramidalizes ( $\tau$ ) and twists ( $\phi$ ) steadily out of plane toward 90°. These structural changes coincide with an overall relaxation of the molecule on  $S_1$ .

indicates that the wavepacket will quickly move away from the nonadiabatic region after population transfer. Thus, the hourglass-like profile for the  $S_1$  (upper) and  $T_2$  (lower) states shown in Figure 4 would usually lead to very efficient quenching of upper-state population. However, because these two states are of different spin, the spin–orbit coupling controls the time scale for population transfer. In nitroarenes, spin–orbit coupling is known to be unusually large, meaning that  $S_1 \rightarrow T_2$  and  $S_1 \rightarrow S_0$  population transfer could compete. The experiments of Takezaki et al.,<sup>12,13</sup> however, showed that population quenching from the  $S_1$  state is dominated by intersystem crossing to  $T_2$  rather than internal conversion to the singlet ground state. This finding is consistent with our calculations, where we observed relatively weak coupling of the  $S_0$  and  $S_1$  states in the nonadiabatic region.

Spin–orbit coupling constants calculated for singlet and triplet electronic state pairs at the  $S_0S_1\text{CI}$  geometries of NB, TNA, and TNT are reported in Table 3. The singlet–triplet coupling constants are quite large when compared to those calculated for other organic molecules:  $9.15 \text{ cm}^{-1}$  for ethylene,  $6.23 \text{ cm}^{-1}$  for benzene,  $4.54 \text{ cm}^{-1}$  for toluene, and  $11.65 \text{ cm}^{-1}$  for pyrrole.<sup>59</sup> By comparison, in the nitroarenes, though the

$S_1/T_2$  couplings are stronger at the  $S_0/S_1$  optimized conical intersection, the  $S_0/T_1$  couplings are also quite significant.

**2,4,6-Trinitroaniline (TNA).** The experimental electronic absorption spectra of solid and solution-phase 2,4,6-trinitroaniline (TNA) are shown Figure 5. In the visible region, the experimental spectra each exhibit a diffuse absorption centered at 3.0 eV. The calculated electronic energy levels of geometry-optimized TNA (TNA-S<sub>0</sub>Min in Figure 6) are given in Table 4. The first excited state of gas-phase TNA is a bright  $\pi\pi^*$  state that is overestimated at 3.7 eV with TD-LC-BLYP. Multireference perturbation theory (MCQDPT) with a SA-2-CAS(12/11) wave function, however, gives an excitation energy of 3.0 eV, in good agreement with the experimental results. The  $S_1$  state is considerably lower in energy than the lowest bright ( $^1\text{CT}$ ) state in nitrobenzene, due to the extension of the  $\pi$ -bonding network by the functional groups, particularly the NH<sub>2</sub>. The  $S_0 \rightarrow S_1$  transition is primarily HOMO  $\rightarrow$  LUMO. These orbitals are

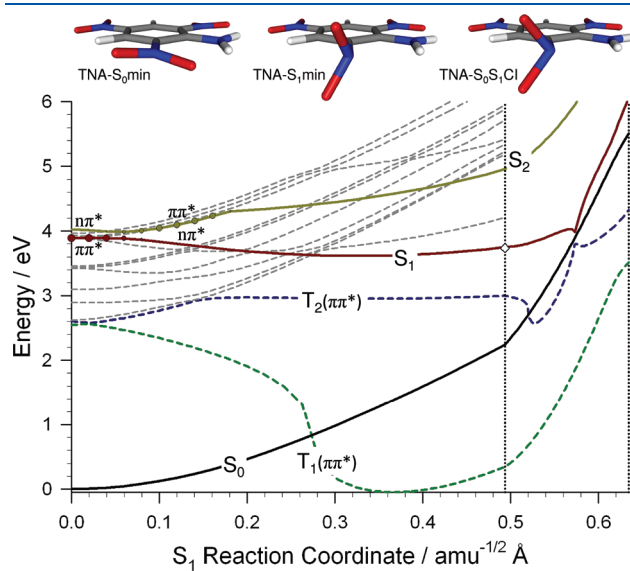


**Figure 9.** Energies (TD-LC- $\omega$ PBE/cc-pVDZ) of the lowest three singlet (solid lines) and lowest 12 triplet (dashed lines) states in TNA along a linearly interpolated RC connecting the ground-state ( $S_0$ ) minimum, the  $S_1$  minimum, and the  $S_0/S_1$  conical intersection, which are shown in Figure 4. The sizes of the filled circles on the  $S_1$  curve are weighted by the  $S_0 \leftrightarrow S_1$  oscillator strength; thus, this plot shows that the  $S_0 \leftrightarrow S_1$  transition darkens with a strongly avoided crossing of  $S_1$  and  $S_2$ . See the legend of Figure 2 for more details.

shown in Figure 7. The HOMO is a benzene-like  $\pi$  MO, whereas the  $\pi^*$  MO is delocalized but has considerable amplitude at the NO<sub>2</sub> functional groups. This situation is similar to what was found for 1,3,5-triamino-2,4,6-trinitrobenzene (TATB)<sup>60</sup> and for the  $^1\text{CT}$  state of nitrobenzene (Figure 2 and ref 46). Promotion of an electron from the HOMO to the LUMO is expected to lead to a loss of bonding character in the benzene ring structure (through reduction of the HOMO occupation by one-half) and also in the NO<sub>2</sub> groups (through increasing antibonding character). In contrast, the second singlet excited state, accessed by a HOMO  $- 1 \rightarrow$  LUMO + 1 (see Figure 7) excitation, is a dark  $n\pi^*$  state with increased C–N  $\pi$ -bonding character for the para NO<sub>2</sub> group. The lowest three triplet excited states are all characterized by NO  $\pi$ -electron excitation, in the Franck–Condon region.

Results of an excited-state MD simulation using the SA-2-CAS(8/7)/6-31G method are plotted in Figure 8. The trajectory began on the  $S_1$  state at the  $S_0$  equilibrium geometry with no kinetic energy, corresponding to the most probable set of initial conditions (the center of the ground-state distribution function). The purpose of conducting this simulation was simply to explore the excited-state potential energy hypersurface in order to determine which areas should be studied in more depth. The MD study shows that TNA relaxes by torsion and pyramidalization of one of the ortho-positioned nitro groups. In addition, one of the N–O bonds on this nitro group stretches to  $\sim 1.65$  Å and thereafter oscillates about 1.45 Å. The  $S_1 - S_0$  energy gap decreases to a minimum value of 0.45 eV in the first 150 fs. The second ortho nitro group (labeled with a subscript b in Figure 8) “planarizes” on  $S_1$  from a slightly nonplanar  $S_0$  geometry and is inconsequential to the molecule’s relaxation process after photoexcitation.

For our CASSCF optimizations of excited-state TNA, we employed a CAS(10/8) active space that (outside of the Franck–Condon region) contained four NO<sub>2</sub>-localized  $\pi$  orbitals, a ring-localized  $\pi$  orbital, and three NO<sub>2</sub>-localized  $\pi^*$  orbitals. Minimization of the  $S_1$  energy yielded a geometry (TNA-S<sub>1</sub>Min, shown in Figure 6) that has one of the ortho nitro groups twisted and pyramidalized. In this region, the  $S_1$  potential energy surface is shallow and diffuse, the electronic character of the state has changed from  $\pi\pi^*$  to  $n\pi^*$ , and the  $S_0 \leftrightarrow S_1$  transition dipole is negligibly small. Thus, according to our calculations, TNA is not expected to fluoresce in the region of the  $S_1$  minimum.

In the Franck–Condon region,  $S_1 (\pi\pi^*)$  is the bright state; however, when the electronic character of the states switches (to  $n\pi^*$ ) at an avoided crossing (where the red and yellow curves approach

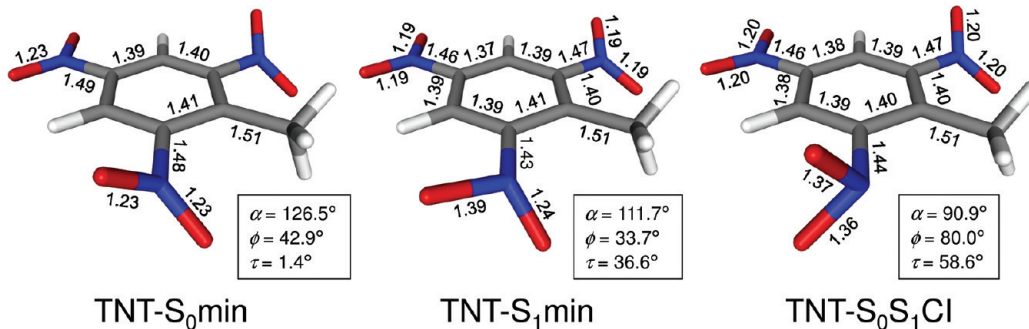


**Figure 10.** Molecular structures at the minima on the ground and first excited states and the minimum-energy  $S_0/S_1$  conical intersection in TNT. The ground-state structure was optimized in  $C_s$  symmetry. Bond lengths are given in angstroms. The torsion ( $\phi$ ) and pyramidalization ( $\tau$ ) angles of the nitro group are described in Scheme 2.

**Table 5.** Electronic Excitation Energies ( $\Delta E$ ) and Oscillator Strengths ( $f$ ) of 2,4,6-Trinitrotoluene (TNT)<sup>a–d</sup>

character	TD-LC- $\omega$ PBE <sup>e</sup>		TD-LC-BLYP <sup>e</sup>		TD-CAM-B3LYP <sup>f</sup>		expt
	$\Delta E$ (eV)	$f$	$\Delta E$ (eV)	$f$	$\Delta E$ (eV)		
$^3A''$ ( $T_1$ )	$\pi\pi^*$	2.36	0	2.77	0		
$^3A'$ ( $T_2$ )	$\pi\pi^*$	2.36	0	2.77	0		
$^3A''$	$\pi\pi^*$	2.41	0	2.79	0		
$^3A'$	$\pi\pi^*$	2.62	0	2.97	0		
$^3A''$	$n\pi^*, \pi\pi^*$	3.27	0	3.22	0		
$^3A''$	$n\pi^*$	3.35	0	3.30	0		
$^3A'$	$n\pi^*, \pi\pi^*$	3.41	0	3.51	0		
$^3A'$	$n\pi^*$	3.74	0	3.74	0		
$^3A''$	$n\pi^*$	3.74	0	3.74	0		
$^3A'$	$n\pi^*$	3.79	0	3.78	0		
$^1A'$ ( $S_1$ )	$n\pi^*, \pi\pi^*$	3.91	0.002	3.80	0.003		
$^1A'''$ ( $S_2$ )	$n\pi^*, \pi\pi^*$	3.92	0.111	3.81	0.014		
$^1A''$ ( $S_3$ )	$n\pi^*$	3.96	0.000	3.86	0.000		
$^3A'$	$\pi\pi^*$	4.33	0	4.27	0		
$^1A'$ ( $S_4$ )	$n\pi^*$	4.35	0.000	4.29	0.001		
$^1A''$ ( $S_5$ )	$n\pi^*$	4.35	0.000	4.29	0.000		
$^1A'$ ( $S_6$ )	$n\pi^*$	4.37	0.000	4.31	0.000		
$^3A''$	$\pi\pi^*$	4.42	0	4.34	0		
$^3A''$	$\pi\pi^*$	4.57	0	4.48	0		
$^1A''$ ( $S_7$ )	$\pi\pi^*$	4.96	0.000	4.77	0.000	5.12	
$^1A'$ ( $S_8$ )	$\pi\pi^*$	5.41	0.124	5.22	0.148	5.51	5.08 <sup>g</sup>
$^3A'$	$\pi\pi^*$	5.78	0	5.51	0		
$^1A''$ ( $S_9$ )	$\pi\pi^*$	5.91	0.217	5.63	0.226	5.58	5.74 <sup>g</sup> , 5.46 <sup>h</sup>
$^3A''$	$\pi\pi^*$	5.98	0	5.70	0		
$^1A'$ ( $S_{10}$ )	$\pi\pi^*$	6.00	0.374	5.72	0.306		
$^1A''$ ( $S_{11}$ )	$\pi\pi^*$	6.33	0.150	6.09	0.047		
$^1A'$ ( $S_{12}$ )	$\pi\pi^*$	6.40	0.152	6.02	0.006		
$^1A''$ ( $S_{13}$ )	$\pi\pi^*$	6.42	0.101	6.28	0.010		
$^3A'$	$\pi\pi^*$	6.51	0	6.24	0		
$^1A'$	$\pi\pi^*$	6.52	0.133	6.31	0.204		
$^1A''$	$\pi\pi^*$	6.66	0.084	6.34	0.107		

<sup>a</sup> TD-DFT calculations performed in  $C_s$  symmetry. <sup>b</sup> TD-CAM-B3LYP calculations taken from ref 46. <sup>c</sup> Character and ordering of the states taken from the TD-LC-BLYP calculations. <sup>d</sup> Results for triplet states given in italics. <sup>e</sup> aug-cc-pVDZ basis set. <sup>f</sup> From ref 62; geometry optimized with B3LYP/cc-pVDZ. <sup>g</sup> Gas phase; ref 18. <sup>h</sup> Ethanol solution; ref 19.

in Figure 9),  $S_1 \rightarrow S_0$  becomes a dark transition. As mentioned earlier, the  $n\pi^*$  orbital is characterized by population of the LUMO + 1 (Figure 8), which includes C–N  $\pi$  bonding at the para position. Thus, out-of-plane NO<sub>2</sub> rotation at the ortho NO<sub>2</sub> group is heavily favored over that of the para-positioned NO<sub>2</sub>.

Because the energy gap decreased significantly along our excited-state MD trajectory, we also searched for an  $S_0/S_1$  nonadiabatic region in the vicinity of the  $S_1$  minimum. The geometry (TNA- $S_0S_1$ Cl, Figure 6) at the conical intersection ( $S_0 - S_1$  energy gap = 0.033 eV) is similar in structure to that of nitrobenzene. As in nitrobenzene, NO<sub>2</sub> pyramidalization and N–O bond elongation are more dramatic in the nonadiabatic region than at the minimum. The nonadiabatic region is 1 eV (Table 2) uphill from the  $S_1$  minimum at the CAS(16/13) level.

The structures of Figure 6 are connected by linear interpolation in Figure 9, where the energies of the lowest three singlet and lowest 12 triplet states are plotted. The approximate RCs of nitrobenzene and TNA show some very similar features as well as some notable differences. First, in both molecules, the

excited-state minimum has  $n\pi^*$  character; thus, little or no fluorescence can be expected in either case. Second, as in NB, three states are nearly degenerate at a point lying near the  $S_0/S_1$  nonadiabatic region predicted by CASSCF. This situation could lead to very interesting excited-state dynamics and the possibility of  $S_1$  population funneling to two very different electronic states. The topographies of the  $S_0$ ,  $S_1$ , and  $T_2$  states surrounding the TNA nonadiabatic region are also very similar to those of NB. A three-dimensional plot of potential energy gaps surrounding this intersection similar to that of NB shown in Figure 4 is given in the Supporting Information. The differences between the surface topographies in NB and TNA are due mainly to the longer N–O bonds in TNA, as well as steric effects present in TNA but not in NB. Finally, there are a large number of triplet electronic states between  $S_0$  and the lowest bright states of both NB and TNA (see Figures 3 and 9). Given the strong spin–orbit couplings calculated for NB and TNA (Table 3), these states could potentially play a significant role in the dynamics following photoexcitation.

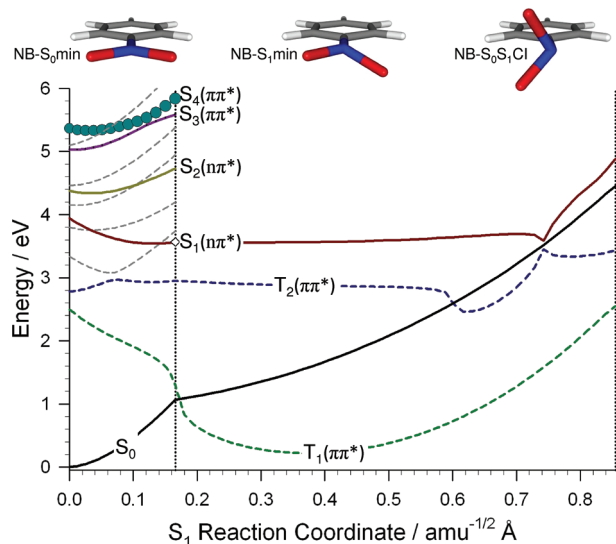


**Figure 11.** Energies (TD-LC- $\omega$ PBE/cc-pVDZ) of the lowest 14 singlet (solid lines) and lowest 15 triplet (dashed lines) states in TNT along a linearly interpolated RC connecting the ground-state ( $S_0$ ) minimum, the  $S_1$  minimum, and the  $S_0/S_1$  conical intersection, which are detailed in Figure 8. See the legend of Figure 2 for more details.

On the other hand, there are two important differences between the first excited states of nitrobenzene and TNA. These both arise from the change in electronic character on  $S_1$  at the avoided crossing near the Franck–Condon region in the latter compound. First, although we found no barrier on  $S_1$ , we cannot rule one out. This is due to two potential deficiencies in our RC study: (1) the  $S_2$ – $S_1$  Franck–Condon energy gap calculated by the TD-LC- $\omega$ PBE method might be underestimated and (2) the minimum-energy path might not exactly coincide with the linearly interpolated RC that we calculated. If either of these is true, a barrier to relaxation on  $S_1$  could exist. Depending on the excitation wavelength, such a barrier might help trap population in the Franck–Condon region to allow radiative decay to  $S_0$ . [The fact that the SA-2-CAS(8/7)/6-31G trajectory described above passes this barrier so easily is at least partly related to the usual overestimation by CASSCF of the Franck–Condon excited-state energy compared with minimum-energy regions of the excited-state surface.] Second, at the  $S_0/S_1$  conical intersection,  $S_1$  is of nπ\* character and connects diabatically to  $S_2$  in the Franck–Condon region. The relative energy of the nonadiabatic region and the Franck–Condon energy of the nπ\*  $S_2$  state is similar to that found in nitrobenzene (which, in that case, is  $S_1$ ). In contrast, according to TD-DFT, the nonadiabatic region is not accessible following  $S_0 \rightarrow S_1$  photoexcitation of TNA. Both of these differences are important in light of the work by Takezaki and co-workers.<sup>12,13</sup> In their experiments, photoexcitation to  $S_1$  of nitrobenzene was found to result in rapid (~100-fs) relaxation on that state, followed by a relatively quick ISC to  $T_2$ . In TNA, because the nonadiabatic region is predicted to be less stabilized compared to the  $S_1$  energy in the Franck–Condon region, a similar intersystem crossing is less likely than in NB. Moreover, if an energy barrier exists on the  $S_1$  adiabat, the initial 100-fs relaxation observed in nitrobenzene should occur with a longer time constant (and possibly smaller quantum yield) in TNA.

**2,4,6-Trinitrotoluene (TNT).** The lowest-energy conformer of TNT is  $C_s$ -symmetric<sup>61</sup> and is pictured in Figure 10. The

ortho-positioned NO<sub>2</sub> groups are rotated out-of-plane to reduce steric repulsion with the methyl group. The electronic excitation energies for the singlet and triplet states of TNT are given in Table 5. The lowest bright state in TNT is  $S_8$  at 5.41 eV using TD-LC- $\omega$ PBE, roughly 0.3 eV higher than the highest-wavelength peak in the gas-phase experimental spectrum.<sup>18</sup> The singly occupied π and π\* MOs for this state are similar to those of S<sub>4</sub> in nitrobenzene (Figure 2) and S<sub>1</sub> in TNA (Figure 7); thus,  $S_8$  can be considered the charge-transfer (CT) state of TNT. Our TD-LC-BLYP excitation energies are in slightly better quantitative agreement with experiment than our TD-LC- $\omega$ PBE results and the TD-CAM-B3LYP results of ref 62; however, all are in good qualitative agreement.

The structures at the  $S_1$  minimum and  $S_0/S_1$  conical intersection ( $S_0$ – $S_1$  energy gap = 0.022 eV) are also shown in Figure 10, with important geometric parameters compared to those of the  $S_0$  minimum. The structures are quite similar to those of nitrobenzene and TNA. An approximate RC connecting the stationary points is plotted in Figure 11. Because the ortho NO<sub>2</sub> groups are twisted out of plane on  $S_0$ , the only motions required for relaxation following excitation to  $S_1$  are alterations in the π-bonding pattern and slight pyramidalization. Accessing the nonadiabatic region then requires further twisting and pyramidalization of the NO<sub>2</sub> group. As in TNA, we found that relaxation on  $S_1$  and access to the nonadiabatic region are both controlled by motion of a single NO<sub>2</sub> group. With this result, important likenesses between Figures 3 and 11, and very similar spin–orbit coupling constants calculated for the two compounds (Table 3), we expect strong similarities between the NB and TNT  $S_1 \rightarrow S_0$  de-excitation pathways.

#### IV. CONCLUSIONS

The electronic states of three important nitroarenes were studied using state-averaged CASSCF and TD-DFT to explore pathways for excited-state decay. Excited- ( $S_1$ -) state minima and  $S_0/S_1$  conical intersection searches were conducted with the CASSCF method, and electronic absorption spectra and  $S_1$  energy relaxation coordinates were computed with TD-DFT. Although we did not search for them directly, we did identify areas where conical intersections between a singlet and triplet state might exist. On the basis of these studies, several important statements can be made.

The experiments of Takezaki et al.,<sup>12,13</sup> in which the dynamics was probed after photoexcitation of NB to  $S_1$ , showed a 100-fs relaxation on  $S_1$  and a 6-ps ISC to the  $T_2$  state. Our quantum chemical results show a relatively flat relaxation coordinate on  $S_1$  leading to a nonadiabatic region involving the  $S_0$ ,  $S_1$ , and  $T_2$  electronic states. Investigation of the topographies of the surfaces surrounding the nonadiabatic regions indicates that, with sufficient spin–orbit coupling, nonradiative quenching from  $S_1$  to  $T_2$  could be preferred over quenching to  $S_0$ . These findings are generally true for TNA and TNT as well. In addition, according to the El-Sayed rules,<sup>7–9</sup> ISC transitions that involve an  $\alpha\beta \rightarrow \alpha\alpha$  spin flip must also involve a change in the orbital angular momentum in order to conserve overall angular momentum. Put another way, spin–orbit coupling between singlet and triplet electronic states should be finite only if the states have different orbital types. All three compounds studied here have nπ\*  $S_1$  states interacting with ππ\*  $T_2$  states in the nonadiabatic region; therefore, spin–orbit coupling between the states should be nonzero, and nonradiative decay from  $S_1$  to  $T_2$  possible. Indeed,

ab initio calculations of spin–orbit coupling of the  $S_1/T_2$  states at the CAS-optimized conical intersections yielded coupling constants that are quite large ( $50\text{--}60\text{ cm}^{-1}$ ) for organic compounds. In addition, the ultrashort time scale for  $T_2 \rightarrow T_1$  decay observed in nitrobenzene implies that a nonadiabatic region exists between the two states. This is consistent with our finding that  $T_1$  and  $T_2$  have similar electronic symmetries (both  $\pi\pi^*$ ) in low-energy sections of their hypersurfaces, away from the Franck–Condon region. Our work also demonstrates that predicting the coupling strength between a singlet state and a triplet state according to the El-Sayed rules requires knowledge of their electronic state (orbital) character in the nonadiabatic region, as these can differ significantly from Franck–Condon character.

In their experiments, Takezaki et al.<sup>12,13</sup> pumped nitrobenzene to the “dark”  $S_1$  state using a  $\sim 2\text{ }\mu\text{J}$  laser pulse and found nonradiative decay of the excited-state population from  $S_1$  to  $S_0$  via the two lowest triplet states.<sup>12,13</sup> Because of the similarities that we calculated between the  $S_0$ ,  $S_1$ ,  $T_1$ , and  $T_2$  potential energy surfaces of nitrobenzene and TNT, we expect population quenching following  $S_0 \rightarrow S_1$  photoexcitation of TNT to occur nonradiatively as well. If the molecule does indeed relax in this fashion, then theoretically, photoexcitation to  $S_1$  would impart  $\sim 88\text{ kcal/mol}$  of heat into a TNT sample and could provide a means for optical initiation.

The lowest-energy bright (charge-transfer) states in NB and TNT are  $S_4$  (5.17 eV)<sup>47,48</sup> and  $S_8$  (5.08 eV),<sup>18</sup> respectively. Ultimately, relaxation from these states could occur by the same mechanism as for  $S_1$  (Kasha’s rule<sup>63</sup>); however, our results are inconclusive. Each compound has both  $n\pi^*$  and  $\pi\pi^*$  triplet states that are lower in energy than the singlet charge-transfer states, making definitive predictions for the de-excitation pathways extremely difficult without further study.

The energy profile that we calculated for the  $S_1$  state of TNA is slightly more complicated than those for NB and TNT. A small activation barrier to relaxation might or might not exist, and the nonadiabatic region is uphill in energy from the Franck–Condon region. As a result, nonradiative quenching of the photoexcited  $S_1$  population should be slower in TNA than in NB and could possibly be shut off entirely with sufficiently high excitation wavelength. If a barrier does exist, it is unlikely that radiative quenching will occur with appreciable quantum efficiency once the barrier has been crossed. However, photon emission might be possible if the wavepacket can be trapped in the Franck–Condon region.

Overall, we found the CASSCF method, and hence all multireference correlation methods as well, to be cumbersome to apply to nitroarenes because of the large number of nonbonding electrons in these compounds. The TD-DFT methods performed better overall, but problems exist when a single-reference method is used for a multireference problem. The ab initio floating-occupation-molecular-orbital SCF + complete-active-space configuration-interaction (FOMO-CAS-CI) method of Slavíček and Martínez<sup>64</sup> holds promise in alleviating these problems by providing a means for calculating global potential energy surfaces for excited electronic states with the quality of a multideterminant method, but at the cost of a single-determinant method. In this technique, a predetermined number of occupied and virtual orbitals are allowed to have non-integer electron occupations (SCF with finite electronic temperature). The non-integer occupations are allowed to adjust instantaneously when the molecular geometry changes. As a result, the (single) reference wave function takes on more mixed-state character near electronic degeneracies. The FOMO SCF is followed by a full CI calculation within the active

orbital space (CAS-CI). These calculations should be particularly useful for nitroarenes, for which a very large number of orbitals are often required to properly describe electronic excitation. They are planned for future studies.

## ■ ASSOCIATED CONTENT

**S Supporting Information.** Cartesian coordinates of the  $S_0$  and  $S_1$  excited-state minima and  $S_0/S_1$  conical intersections of NBN, TNA, and TNT and reduced-space potential energy surfaces for TNA (similar to that shown for NB in Figure 4). This material is available free of charge via the Internet at <http://pubs.acs.org>.

## ■ AUTHOR INFORMATION

### Corresponding Author

\*Phone: 1-781-273-4770. E-mail: jasonq@spectral.com.

## ■ ACKNOWLEDGMENT

The authors thank Todd J. Martínez and Joshua D. Coe for helpful discussions on the manuscript. This work was supported by a Laboratory Directed Research and Development award at Los Alamos National Laboratory (LANL). LANL is managed by Los Alamos National Security, LLC, under U.S. Department of Energy Contract DE-AC52-06NA25396.

## ■ REFERENCES

- (1) Moore, D. S. *Rev. Sci. Instrum.* **2004**, *75*, 2499.
- (2) Greenfield, M.; McGrane, S. D.; Moore, D. S. *J. Phys. Chem. A* **2009**, *113*, 2333.
- (3) McGrane, S. D.; Scharff, R. J.; Greenfield, M.; Moore, D. S. *New J. Phys.* **2009**, *11*, 105047.
- (4) Yu, H. *J. Environ. Sci. Health C* **2002**, *120*, 149.
- (5) Parmenter, C. S. *Adv. Chem. Phys.* **1972**, *22*, 365.
- (6) Ohtani, H.; Kobayashi, T.; Suzuki, K.; Nagakura, S. *Bull. Chem. Soc. Jpn.* **1980**, *53*, 43.
- (7) Lower, S. K.; El-Sayed, M. A. *Chem. Rev.* **1966**, *66*, 199.
- (8) El-Sayed, M. A. *J. Chem. Phys.* **1962**, *36*, 573.
- (9) El-Sayed, M. A. *J. Chem. Phys.* **1963**, *38*, 2834.
- (10) Crespo-Hernández, C. E.; Burdzinski, G.; Arce, R. *J. Phys. Chem. A* **2008**, *112*, 6313.
- (11) Reiser, A.; Leyshon, L. J.; Saunders, D.; Mijovic, M. V.; Bright, A.; Brogie, J. *J. Am. Chem. Soc.* **1972**, *94*, 2414.
- (12) Takezaki, M.; Hirota, N.; Terazima, M. *J. Phys. Chem. A* **1997**, *101*, 3443.
- (13) Takezaki, M.; Hirota, N.; Terazima, M. *J. Chem. Phys.* **1998**, *108*, 4685.
- (14) Zugazagoitia, J. S.; Almora-Díaz, C. X.; Peón, J. *J. Phys. Chem. A* **2008**, *112*, 358.
- (15) Khalil, O. S.; Bach, H. G.; McGlynn, S. P. *J. Mol. Spectrosc.* **1970**, *35*, 455.
- (16) Seliskar, C. J.; Khalil, O. S.; McGlynn, S. P. In *Excited States*; Lim, E. C., Ed.; Academic Press: New York, 1974; Vol. I.
- (17) Cooper, P. W. *Explosives Engineering*; Wiley-VCH: New York, 1996.
- (18) Usachev, A. D.; Miller, T. S.; Singh, J. P.; Yueh, F.-Y.; Jang, P.-R.; Monts, D. L. *Appl. Spectrosc.* **2001**, *55*, 125.
- (19) Schroeder, W. A.; Silcox, P. E.; Trueblood, K. N.; Dekker, A. O. *Anal. Chem.* **1951**, *23*, 1740.
- (20) Dunning, T. H. *J. Chem. Phys.* **1989**, *90*, 1007.
- (21) Tawada, Y.; Tsuneda, T.; Yanagisawa, S.; Yanai, T.; Hirao, K. *J. Chem. Phys.* **2004**, *120*, 8425.
- (22) Vydrov, O. A.; Scuseria, G. E. *J. Chem. Phys.* **2006**, *125*, 234109.

- (23) Heyd, O. A. V. J.; Krukau, A.; Scuseria, G. E. *J. Chem. Phys.* **2006**, *125*, 074106.
- (24) Vydrov, O. A.; Scuseria, G. E.; Perdew, J. P. *J. Chem. Phys.* **2009**, *126*, 154109.
- (25) Frisch, M. J.; Trucks, G. W.; Schlegel, H. B.; Scuseria, G. E.; Robb, M. A.; Cheeseman, J. R.; Scalmani, G.; Barone, V.; Mennucci, B.; Petersson, G. A.; Nakatsuji, H.; Caricato, M.; Li, X.; Hratchian, H. P.; Izmaylov, A. F.; Bloino, J.; Zheng, G.; Sonnenberg, J. L.; Hada, M.; Ehara, M.; Toyota, K.; Fukuda, R.; Hasegawa, J.; Ishida, M.; Nakajima, T.; Honda, Y.; Kitao, O.; Nakai, H.; Vreven, T.; Montgomery, J. A., Jr.; Peralta, J. E.; Ogliaro, F.; Bearpark, M.; Heyd, J. J.; Brothers, E.; Kudin, K. N.; Staroverov, V. N.; Kobayashi, R.; Normand, J.; Raghavachari, K.; Rendell, A.; Burant, J. C.; Iyengar, S. S.; Tomasi, J.; Cossi, M.; Rega, N.; Millam, J. M.; Klene, M.; Knox, J. E.; Cross, J. B.; Bakken, V.; Adamo, C.; Jaramillo, J.; Gomperts, R.; Stratmann, R. E.; Yazyev, O.; Austin, A. J.; Cammi, R.; Pomelli, C.; Ochterski, J. W.; Martin, R. L.; Morokuma, K.; Zakrzewski, V. G.; Voth, G. A.; Salvador, P.; Dannenberg, J. J.; Dapprich, S.; Daniels, A. D.; Farkas, Ö.; Foresman, J. B.; Ortiz, J. V.; Cioslowski, J.; Fox, D. J. *Gaussian 09, Revision A.1*; Gaussian, Inc., Wallingford CT, 2009.
- (26) Becke, A. D. *Phys. Rev. A* **1988**, *38*, 3098.
- (27) Lee, C.; Yang, W.; Parr, R. G. *Phys. Rev. B* **1988**, *37*, 785.
- (28) Tawada, Y.; Tsuneda, T.; Yanagisawa, S.; Yanai, Y.; Hirao, K. *J. Chem. Phys.* **2004**, *120*, 8425.
- (29) Iikura, H.; Tsuneda, T.; Yanai, T.; Hirao, K. *J. Chem. Phys.* **2001**, *115*, 3540.
- (30) Frisch, M. J.; Trucks, G. W.; Schlegel, H. B.; Scuseria, G. E.; Robb, M. A.; Cheeseman, J. R.; Montgomery, J. A., Jr.; Vreven, T.; Kudin, K. N.; Burant, J. C.; Millam, J. M.; Iyengar, S. S.; Tomasi, J.; Barone, V.; Mennucci, B.; Cossi, M.; Scalmani, G.; Rega, N.; Petersson, G. A.; Nakatsuji, H.; Hada, M.; Ehara, M.; Toyota, K.; Fukuda, R.; Hasegawa, J.; Ishida, M.; Nakajima, T.; Honda, Y.; Kitao, O.; Nakai, H.; Klene, M.; Li, X.; Knox, J. E.; Hratchian, H. P.; Cross, J. B.; Bakken, V.; Adamo, C.; Jaramillo, J.; Gomperts, R.; Stratmann, R. E.; Yazyev, O.; Austin, A. J.; Cammi, R.; Pomelli, C.; Ochterski, J. W.; Ayala, P. Y.; Morokuma, K.; Voth, G. A.; Salvador, P.; Dannenberg, J. J.; Zakrzewski, V. G.; Dapprich, S.; Daniels, A. D.; Strain, M. C.; Farkas, O.; Malick, D. K.; Rabuck, A. D.; Raghavachari, K.; Foresman, J. B.; Ortiz, J. V.; Cui, Q.; Baboul, A. G.; Clifford, S.; Cioslowski, J.; Stefanov, B. B.; Liu, G.; Liashenko, A.; Piskorz, P.; Komaromi, I.; Martin, R. L.; Fox, D. J.; Keith, T.; Al-Laham, M. A.; Peng, C. Y.; Nanayakkara, A.; Challacombe, M.; Gill, P. M. W.; Johnson, B.; Chen, W.; Wong, M. W.; Gonzalez, C.; Pople, J. A. *Gaussian 03, revision C.02*; Gaussian, Inc.: Wallingford, CT, 2004.
- (31) Nakano, H. *J. Chem. Phys.* **1993**, *99*, 7983.
- (32) Nakano, H. *Chem. Phys. Lett.* **1993**, *207*, 372.
- (33) Bearpark, M. J.; Robb, M. A.; Schlegel, H. B. *Chem. Phys. Lett.* **1994**, *223*, 269.
- (34) Ragazos, I. N.; Robb, M. A.; Bernardi, F.; Olivucci, M. *Chem. Phys. Lett.* **1992**, *197*, 217.
- (35) Bernardi, F.; Robb, M. A.; Olivucci, M. *Chem. Soc. Rev.* **1996**, *25*, 321.
- (36) Adamo, C.; Barone, V. *J. Chem. Phys.* **1999**, *110*, 6158.
- (37) Gordon, M. S.; Schmidt, M. W. *Theory and Applications of Computational Chemistry: The First Forty Years*; Dykstra, C. E., Frenking, G., Kim, K. S., Scuseria, G. E., Eds.; Elsevier: Amsterdam, 2005.
- (38) Schmidt, M. W.; Baldridge, K. K.; Boatz, J. A.; Elbert, S. T.; Gordon, M. S.; Jensen, J. H.; Koseki, S.; Matsunaga, N.; Nguyen, K. A.; Su, S.; Windus, T. L.; Dupuis, M.; Montgomery, J. A. *J. Comput. Chem.* **1993**, *14*, 1347.
- (39) Swope, W. C.; Anderson, H. C.; Berens, P. H.; Wilson, K. R. *J. Chem. Phys.* **1982**, *76*, 637.
- (40) Dreuw, A.; Head-Gordon, M. *Chem. Rev.* **2005**, *105*, 4009.
- (41) Burke, K.; Werschnik, J.; Gross, E. K. U. *J. Chem. Phys.* **2005**, *123*, 062206.
- (42) Levine, B. G.; Ko, C.; Quenneville, J.; Martínez, T. J. *Mol. Phys.* **2006**, *104*, 1039.
- (43) Minezawa, N.; Gordon, M. S. *J. Phys. Chem. A* **2009**, *113*, 12749.
- (44) Fedorov, D. G.; Gordon, M. S. *J. Chem. Phys.* **2000**, *112*, 5611.
- (45) Fedorov, D. G.; Koseki, S.; Schmidt, M. W.; Gordon, M. S. *Int. Rev. Phys. Chem.* **2003**, *22*, 551.
- (46) Kröhl, O.; Malsch, K.; Swiderek, P. *Phys. Chem. Chem. Phys.* **2000**, *2000*, 947.
- (47) Nagakura, S.; Kojima, M.; Maruyama, Y. *J. Mol. Spectrosc.* **1964**, *13*, 174.
- (48) Robin, M. R. *Higher Excited States of Polyatomic Molecules*; Academic Press: New York, 1975; Vol. II.
- (49) Takezaki, M.; Hirota, N.; Terazima, M.; Sato, H.; Nakajima, T.; Kato, S. *J. Phys. Chem. A* **1997**, *101*, 5190.
- (50) Coe, J. D.; Martínez, T. J. *J. Phys. Chem. A* **2006**, *110*, 618.
- (51) Kistler, K. A.; Matsika, S. *J. Chem. Phys.* **2008**, *128*, 215102.
- (52) Matsika, S. *Chem. Phys.* **2008**, *349*, 356.
- (53) Matsika, S. *J. Phys. Chem. A* **2005**, *109*, 7538.
- (54) Matsika, S.; Yarkony, D. R. *J. Am. Chem. Soc.* **2003**, *125*, 12428.
- (55) Matsika, S.; Yarkony, D. R. *J. Am. Chem. Soc.* **2003**, *125*, 10672.
- (56) Matsika, S.; Yarkony, D. R. *J. Chem. Phys.* **2002**, *117*, 6907.
- (57) Matsika, S.; Yarkony, D. R. *J. Phys. Chem. B* **2002**, *106*, 8108.
- (58) Yarkony, D. R. *J. Chem. Phys.* **2001**, *114*, 2601.
- (59) Gogan, S.; Haas, Y.; Zilberg, S. *J. Photochem. Photobiol. A* **2007**, *190*, 200.
- (60) Wu, C. J.; Yang, L. H.; Fried, L. E.; Quenneville, J.; Martínez, T. J. *Phys. Rev. B* **2003**, *67*, 235101.
- (61) Clarkson, J.; Smith, W. E.; Batchelder, D. N.; Smith, D. A.; Coats, A. M. *J. Mol. Struct. (THEOCHEM)* **2003**, *648*, 203.
- (62) Mohammed, A.; Ågren, H.; Norman, P. *Phys. Chem. Chem. Phys.* **2009**, *11*, 4539.
- (63) Kasha, M. *Faraday Discuss.* **1950**, *9*, 14.
- (64) Slavíček, P.; Martínez, T. J. *J. Chem. Phys.* **2010**, *132*, 234102.